HOKKAIDO UNIVERSITY

Title	Histochemical assessment of the anabolic effects of abaloparatide on the femoral metaphyses of ovariectomized mice
Author(s)	Liu, Xuanyu; Hasegawa, Tomoka; Sakakibara, Mako et al.
Citation	Journal of oral biosciences, 67(2), 100663 https://doi.org/10.1016/j.job.2025.100663
Issue Date	2025-04-18
Doc URL	https://hdl.handle.net/2115/97810
Rights	©2025. This manuscript version is made available under the CC-BY-NC-ND 4.0 license https://creativecommons.org/licenses/by-nc-nd/4.0/
Rights(URL)	https://creativecommons.org/licenses/by-nc-nd/4.0/
Type	journal article
File Information	2025.4.10._JOB_Liu_et_al_revised_manuscript.pdf

Hokkaido University Collection of Scholarly and Academic Papers : HUSCAP

Histochemical assessment of the anabolic effects of abaloparatide on the femoral metaphyses of ovariectomized mice

Xuanyu Liu[1,2], Tomoka Hasegawa[1§], Mako Sakakibara[1], Tomomaya Yamamoto[1,4], Mai Haraguchi-Kitakamae[1], Hotaka Ishizu[1,3], Yan Shi[1], Jiaxin Cui[1], Weisong Li[1], Wang Haoyu[1], Hiromi Hongo[1], Tomohiro Shimizu[3], Yoichi Ohiro[2], Norio Amizuka[1]

[1]Ultrastructure of Hard Tissue, [2]Oral and Maxillofacial Surgery, Faculty of Dental Medicine, Hokkaido University, Sapporo, Japan, [3]Orthopaedic Surgery, Faculty of Medicine, Hokkaido University, Sapporo, Japan, [4]Department of Dentistry, Japan Ground Self-Defense Force, Camp Shinmachi, Japan,

Running Headline/Short Title: Abaloparatide-driven anabolic effects

§ Corresponding Author

Tomoka Hasegawa, DDS, Ph.D.

Ultrastructure of Hard Tissue,

Graduate School of Dental Medicine,

Faculty of Dental Medicine, Hokkaido University

Kita 13, Nishi 7, Kita-Ku, Sapporo,

Hokkaido, 060-8586, Japan

Tel/fax: +81-11-706-4226

E-mail: hasegawa@den.hokudai.ac.jp

Abstract

Objective: To clarify the mechanism of bone anabolism induced by the parathyroid hormone-related peptide analog abaloparatide, we histochemically examined the femora of ovariectomized mice treated with abaloparatide.

Methods: Twelve-week-old female C57BL/6J mice underwent ovariectomies (OVX), and were then administered either abaloparatide (30 μg/kg/day: OVX+ABL group) or vehicle (OVX group) via daily intraperitoneal injection. Femora were harvested at 0, 2, 4, and 6 weeks post-administration and subjected to micro-CT imaging, TRAP, cathepsin K, ALP, and PHOSPHO1 staining, along with calcein labeling.

Results: In the OVX group, trabecular number and bone volume gradually decreased over time, whereas the OVX + ABL group maintained these values to 6 weeks after OVX. The numbers of TRAP-positive/cathepsin K-reactive osteoclasts per bone surface area were similar between the OVX and OVX + ABL group, except for a temporary increase at 4 weeks in the OVX group. In the OVX group, the areas of ALP-positive osteoblastic cells and PHOSPHO1-reactive mature osteoblasts decreased, whereas in the OVX+ABL group, ALP-positive osteoblastic cells surrounded the trabeculae, and long lines of PHOSPHO1-reactive mature osteoblasts expanded to the terminal region of the trabeculae. In

addition, long continuous calcein labeling was seen on slightly convex new bone, indicating modeling-based bone formation in the OVX + ABL group. The bone formation rate/bone surface ratio and the total length of modeling-based bone formation sites were higher in the OVX + ABL group than in the OVX group.

Conclusion: Abaloparatide suppresses bone loss following ovariectomy by promoting both remodeling-based and modeling-based bone formation.

247 words

Key words: abaloparatide, bone formation, bone histomorphometry, osteoblast, osteoclast

1. Introduction

Abaloparatide, a novel 34 amino acid peptide analog of the parathyroid hormone-related peptide (PTHrP), is an anabolic agent used for osteoporosis treatment. In the amino acid sequence of abaloparatide, residues 22, 23, 25, 26, 28, 29, 30, 31, and 34 of the authentic PTHrP were substituted with Glu, Leu, Glu, Lys, Leu, 2-methylAla, Lys, Leu, and Ala-NH2, respectively, making them stable synthetic peptides *in vivo*. Although the amino acid structures of the two peptides differ significantly, abaloparatide is thought to stimulate the parathyroid hormone(PTH)/PTHrP receptor and exert a bone anabolic effect when administered intermittently [1].

Abaloparatide was approved by the Food and Drug Administration in April 2017 for the treatment of severe osteoporosis. The Abaloparatide Comparator Trial in Vertebral Endpoints (ACTIVE), a phase III clinical trial in postmenopausal women with osteoporosis, showed that daily subcutaneous injections of abaloparatide significantly increased bone mineral density (BMD) in the lumbar spine, hip, and femoral neck and reduced the risk of vertebral and non-vertebral fractures compared to placebo and teriparatide administration [2-4]. Recently, Matsumoto et al. examined whether the favorable anabolic effects of abaloparatide observed in the ACTIVE trial are also observed in Japanese patients [5]. They concluded that in postmenopausal Japanese female patients, as well as male patients with osteoporosis with a high fracture risk, abaloparatide administration robustly increased BMD in the lumbar spine, total hip, and femoral neck, suggesting a similar efficacy in

Japanese patients. More recently, in the Abaloparatide for the Treatment of Men with Osteoporosis (ATOM) trial, male patients with primary or hypogonadism-associated osteoporosis received subcutaneous injections of abaloparatide or a placebo [6], and which induced significant and rapid improvements in BMD. These findings suggest that abaloparatide stimulates bone formation with a minimal increase in bone resorption, resulting in a larger net bone anabolic window. Therefore, there appears to be, at least to some extent, a difference in the anabolic effects of teriparatide and abaloparatide when they are used for osteoporotic treatment.

Many histomorphometric and marker analyses have been performed using osteoporotic rodent models to better understand the mechanisms underlying abaloparatide-driven anabolic effects. Sprague–Dawley rats subjected to ovariectomy (OVX) show bone loss after 3 months, and abaloparatide treatment increases bone mass, strength, and quality in these rats[1]. Other studies have reported that skeletal restoration is associated with improved trabecular microarchitecture, cortical geometry, and bone strength in abaloparatide-treated OVX rats [7]. However, few studies have provided histological evidence *in vivo* in osteoporotic rodent models treated with abaloparatide. Recently, Makino et al. characterized the femoral histology of mice administered teriparatide or abaloparatide, and verified that abaloparatide induced stronger anabolic effects than teriparatide [8]. However, they did not employ an OVX-induced osteoporosis model; thus, it is necessary to investigate whether and how abaloparatide inhibits osteoporosis in mice.

To better understand how abaloparatide inhibits osteoporosis, we examined the femora of OVX mice, with and without abaloparatide administration, using immunohistochemical and bone histomorphometric analyses.

2. Materials and Methods

2.1. Animals

Twelve-week-old female C57BL/6J mice (n = 48; Japan CLEA, Tokyo, Japan) were handled according to Hokkaido University's guidelines for animal care and research use (approved study protocol #23-0096). All the mice underwent OVX, and then abaloparatide (#4105586, Bachem Holding AG, Bubendorf, Switzerland; 30 μg/kg/day; OVX+ABL group, n = 24) or the vehicle (OVX group, n = 24) was intraperitoneally administered once daily for 6 weeks, with femora samples examined at 0 (immediately after the administration of abaloparatide or the vehicle), 2, 4, and 6 weeks.

2.2. Specimen preparation

For bone labeling, the mice were injected subcutaneously with 20 mg/kg of 0.1% calcein solution 1 and 3 days before sacrifice. They were fixed with 4% paraformaldehyde in 0.1 M phosphate buffer (pH 7.4) through the left ventricle after anesthetization using an intraperitoneal injection of a combination of anesthetic agents: 0.3 mg/kg of medetomidine, 4.0 mg/kg of midazolam, and 5.0 mg/kg

of butorphanol. Femora were removed and then immersed in the same fixative for 24 h. Then, the left femora were soaked in 0.1 M phosphate-buffered saline (PBS) prior to micro-computed tomography (micro-CT) analyses. The left femora were decalcified with 10% ethylenediaminetetraacetic disodium salt for 2 months at 4 °C prior to paraffin embedding. Five μm-thick sagittal sections were cut parallel to the bone's longitudinal axis. Calcein labeling was performed at weeks 0, 2, and 6 The right femora were immersed in 70% ethanol, perfused for 18 h, and embedded in methyl methacrylate. Paraffin-embedded sections were subjected to histochemical staining as described in the next section. All sections were photographed under a Nikon Eclipse E800 microscope (Nikon Instruments Inc., Tokyo, Japan) equipped with a digital camera (Nikon DXM1200C, Nikon).

2.3. Micro-CT analysis

Micro-CT images of the left femora were obtained using a micro-CT unit (CosmoScan FX, Rigaku Corporation, Tokyo, Japan) with the following parameters: tube voltage 90 kV, tube current 88 μA, and field of view (FOV) 10 mm, as described in our recent report [9].

2.4. Immunohistochemistry for cathepsin K, ALP, and PHOSPHO1

The dewaxed paraffin sections were immersed in 0.3% H_2O_2 in PBS for 30 min to block endogenous peroxidase activity. To reduce nonspecific binding, 1% bovine serum albumin (Serologicals Proteins Inc., Kankakee, IL, USA) in PBS (1% BSA-PBS) was added to the sections for 20 min. The treated

sections were incubated with mouse anti-human cathepsin K (Daiichi Fine Chemical Co., Ltd., Takaoka, Japan) in 1% BSA-PBS at a dilution of 1:200 at room temperature (RT) for 2 h [10], and then with horseradish peroxidase (HRP)-conjugated anti-mouse IgG (Chemicon International Inc., Temecula, CA). For the detection of tissue nonspecific alkaline phosphatase (ALP) and phosphoethanolamine/phosphocholine phosphatase 1 (PHOSPHO1), sections were incubated with rabbit polyclonal antiserum against ALP [11] in 1% BSA-PBS (1:300) and rabbit polyclonal anti-PHOSPHO1 (Cusabio Technology Llc., Houston, TX) [12] in 1% BSA-PBS (1:100) for 2h, respectively, and then with HRP-conjugated goat anti-rabbit IgG (DakoCytomation, Glostrup, Denmark) at a dilution of 1:100 for 1 h at RT. To visualize all HRP-conjugated immunoreactions, diaminobenzidine tetrahydrochloride was used as the substrate. All sections were counterstained with methyl green and observed under a light microscope.

2.5. Enzyme histochemistry for tartrate-resistant acid phosphatase

Tartrate-resistant acid phosphatase (TRAP) was detected as previously described [13]; in short, dewaxed paraffin sections were rinsed with PBS and incubated in a mixture of 2.5 mg of naphthol AS-BI phosphate (Sigma-Aldrich St. Louis, MO), 18 mg of red violet LB salt (Sigma-Aldrich), and 100 mM L(+) tartaric acid (0.76 g, Nacalai Tesque, Inc., Kyoto, Japan) diluted in 30 ml of a 0.1 M sodium acetate buffer (pH 5.0) for 15 min at 37 °C.

156 *2.6. Selection of the regions of interest (ROIs) in metaphyses for statistical analyses*

157 The assumed rectangular 600 (width) × 1200 (height) μm areas located just below the growth plate
158 positioned horizontally at a 1:3 ratio closer to the femoral anterior were selected as regions of interest
159 (ROI) in the femoral metaphysis for analyses of static bone histomorphometry, TRAP-
160 positive/cathepsin K-reactive osteoclast number, and ALP-positive and PHOSPHO1-reactive areas [9].
161 However, for analyzing the dynamic parameters (calcein labeling) of bone histomorphometry, we
162 divided this rectangular ROI into two regions—assumed square 600 (width) × 600 (length) μm areas
163 located just below the growth plate (the close region) and immediately diaphysis-ward of this proximal
164 region (the distant region) of the ROI.

165

166 *2.7. Quantification of bone histomorphometric parameters and immunohistochemistry in the ROIs*

167 In the metaphyseal rectangular 600 × 1200 μm ROIs, bone volume (BV)/tissue volume (TV),
168 trabecular number (Tb.N), trabecular thickness (Tb.Th.), trabecular separation (Tb.Sp.) The TRAP-
169 positive osteoclast numbers/TV (TRAP-Oc. N/TV), and cathepsin K-reactive osteoclast numbers/TV
170 (Cat K-Oc.N/TV) and TRAP-positive osteoclast numbers/bone surface (BS) (TRAP-Oc. N/BS), and
171 cathepsin K-reactive osteoclast numbers/BS (Cat K-Oc.N/BS), ALP-positive area/TV (ALP+area/TV),
172 ALP-positive area/BV (ALP+area/BV), PHOSPHO1-reactive area/TV (PHOSPHO1+area/TV), and
173 PHOSPHO1-reactive area/BV (PHOSPHO1+area/BV) were determined using Image-Pro Plus 6.2
174 (Media Cybernetics, Inc., Bethesda, MD, USA), as reported by Hasegawa et al. [14]. Whenever

possible, the abbreviations and calculations were performed according to the recommendations of the ASBMR Histomorphometry Nomenclature Committee [15]. To analyze double calcein labeling in the close and distant ROIs, we examined the average length of calcein double labeling and bone formation rate (BFR)/BS according to Haraguchi-Kitakamae et al. [16], as well as the total length of both modeling and remodeling sites six weeks after performing OVX, as recently reported by Hasegawa et al. [14] in the two proximal and distal ROIs. To distinguish between the remodeling and modeling sites, we followed our recent report [14]. In brief, a calcein label (second labeling) appearing over a scalloped label (first labeling) in the new bone was identified as the remodeling site, indicating bone formation following bone resorption. Conversely, a mildly convex calcein label (second labeling) appearing over a smooth calcein label (first labeling) was identified as the modeling site.

2.8. Statistical analysis

All values are presented as mean ± standard deviation (SD). Shapiro–Wilk tests were conducted to assess normality. For normally distributed data, Student's t-tests were used to compare two groups, whereas one-way analysis of variance (ANOVAs) was used to compare multiple time points (0, 2, 4, and 6 weeks). When one-way ANOVAs indicated significant differences between means, simple effect analyses were performed using Fisher's least significant difference (LSD) test. For all tests, P-values < 0.05 were considered significant.

3. Results

3.1. Micro-CT images and histological and bone histomorphometric parameters

Micro-computed tomography (micro-CT) demonstrated a gradual reduction in metaphyseal trabeculae in the OVX group until 6 weeks after OVX **(Fig. 1A–D)**. In contrast, more metaphyseal trabeculae were observed in the femora of abaloparatide-treated mice than in those of OVX mice of the same age **(Fig. 1E–H)**. Consistent with the micro-CT images, the femoral metaphyses of the OVX group clearly deteriorated over time in the histological imagery **(Fig. 2A–H)**, whereas those of the OVX + ABL group did not change **(Fig. 2I–P)**. Bone histomorphometry revealed significantly higher BV/TV, Tb.Th, and Tb.N values in the OVX + ABL group than those in the OVX group **(Fig. 2Q–S)**. Conversely, Tb.Sp were consistently and significantly lower in the abaloparatide group **(Fig. 2T)**. Thus, abaloparatide administration inhibited the deterioration of the metaphyseal trabeculae that accompanies OVX in mice.

3.2. Distribution of TRAP-positive/cathepsin K-reactive osteoclasts

Immediately after vehicle administration (0 week), TRAP-positive/cathepsin K-reactive osteoclasts in the femora of OVX-group mice were scattered throughout the metaphyseal trabeculae **(Fig. 3A, I)**. Thereafter, the number of TRAP-positive/cathepsin K-reactive osteoclasts decreased as the metaphyseal trabeculae diminished over time **(Fig. 3B–D, J–L)**. In the OVX + ABL group, unlike in

the OVX group, the scattered distribution of TRAP-positive/cathepsin K-reactive osteoclasts remained similar throughout the experimental period **(Fig. 3E–H, M–P)**. Bone histomorphometric analysis showed higher values of the TRAP-Oc.N/TV and Cat K-Oc.N/TV in the OVX + ABL group **(Fig. 3Q, S)**. However, when examining the number of osteoclasts per bone surface area, no significant differences were observed between the OVX and OVX + ABL groups for TRAP-Oc. N/BS and Cat K-Oc.N/BS **(Fig. 3R, T)**; however, the OVX group showed higher values for both measures at 4 weeks.

3.3. Distribution of ALP-positive and PHOSPHO1-reactive osteoblasts

Next, we examined the distribution of ALP-positive osteoblasts, including pre-osteoblasts, and PHOSPHO1-reactive mature osteoblasts. In both the treatment groups, ALP-positive osteoblasts surrounded the metaphyseal trabeculae immediately after OVX **(Fig. 4A, E, I, M)**. Consistent with the decrease in metaphyseal trabeculae, the OVX group showed a gradual reduction in ALP-immunoreactive areas **(Fig. 4B–D, F–H)**. In contrast, the OVX + ABL group exhibited increased ALP immunoreactivity covering the metaphyseal trabeculae throughout the experimental period **(Fig. 4J–L, N–P)**. Statistical analysis revealed significantly higher values of both ALP+area/TV and ALP+area/BV in the OVX + ABL group beginning 2 weeks post-operation **(Fig. 4Q, R)**. Thus, the area of ALP-immunopositive osteoblastic cells increased in the femoral metaphysis following abaloparatide administration.

Next, we examined the distribution of PHOSPHO1, a novel phosphatase that plays an important role in increasing the Pi/PPi ratio within matrix vesicles secreted by bone-mineralizing mature osteoblasts. [17-19]. In the OVX group, PHOSPHO1-reactive mature osteoblasts were primarily observed in the metaphyseal trabeculae near the chondroosseous junction **(Fig. 5A, E)**. Along with the decrease in metaphyseal trabeculae following OVX, the localization of PHOSPHO1-reactive osteoblasts was increasingly restricted to the chondro-osseous junction **(Fig. 5B–D, F–H)**. Immediately after OVX, PHOSPHO1-reactive mature osteoblasts in the femora of the OVX + ABL group showed a distribution similar to that of the OVX group **(See Fig. 5A, E, I, M)**, but as time progressed, many rows of PHOSPHO1-reactive osteoblasts were observed, forming lines extending even into the terminal region of the trabeculae **(Fig. 5J–L, N–P)**. Statistical analysis demonstrated significantly greater PHOSPHO1+area/TV at 2, 4, and 6 weeks after treatment initiation and PHOSPHO1+area/BV at 2 and 6 weeks in the OVX + ABL group than in the OVX group **(Fig. 5Q, R)**. Thus, the area of PHOSPHO1-reactive mature osteoblasts, which are indicative of bone-mineralizing osteoblasts, increased in the femoral metaphyses following abaloparatide administration.

3.4. Calcein labeling in the femoral metaphyses

We examined the distribution of calcein labeling to visualize mineralization in two specific ROIs: the closed region, located just beneath the growth plate, and the distant region, directly in the diaphysis ward of the proximal region **(Fig. 6A, B)**. Immediately after OVX, there was no difference in the

distribution of calcein labeling between the close and distant regions, or between the OVX + ABL and OVX groups **(Fig. 6C, F, I, L)**. In the closed ROI, the calcein-labeled areas shortened over time in the OVX group **(Fig. 6D, E)**, whereas many continuous, long calcein-positive areas were observed in the OVX + ABL group **(Fig. 6G, H)**. In the distant ROIs, longer lines of calcein labeling were observed in the OVX + ABL group **(Fig. 6M, N)** while they appeared to diminish in the OVX group **(Fig. 6J, K)**. In particular, long continuous convex double labeling of calcein was observed in the OVX + ABL group, indicating the formation of new convex bone through modeling-based bone formation **(Fig. 6N)**.

Bone histomorphometric analysis demonstrated that the average length of calcein labeling was significantly longer in the OVX+ABL group than in the OVX group in both the close and distant ROIs at 6 weeks **(Fig. 7A, B)**. Likewise, the BFR/BS was significantly greater in the OVX+ABL group at 6 weeks in the closed region and at 2 and 6 weeks in the distant region **(Fig. 7C, D)**. The total length of the remodeling sites was higher in the OVX + ABL group than in the OVX group in the closed ROI 6 weeks after OVX; however, no significant differences were detected in the distant ROI **(Fig. 7E, F)**. However, the length of the modeling sites was significantly greater in the OVX + ABL group than in the OVX group at 6 weeks in both ROIs **(Fig. 7G, H)**.

4. Discussion

In this study, abaloparatide administration at 30 μg/kg once daily for 6 weeks to OVX mice increased bone mass in the femoral metaphyses due to stimulation of bone formation that exceeded bone resorption. When we measured TRAP-Oc. N/TV and Cat K-Oc.N/TV within the ROI of the femoral metaphyses; the OVX + ABL group exhibited the highest values. However, when these values were converted from numbers per BV to numbers per BS, there were no consistent overall significant differences in the number of osteoclasts numbers/BS between groups. In contrast, ALP+area/TV, ALP+area/BV, PHOSPHO1+area/TV, and PHOSPHO1+area/BV were significantly higher and PHOSPHO1-reactive osteoblasts formed long lines to the trabecular termini in the OVX + ABL group. When the ROI in the femoral metaphyses was divided into close and distant regions, the calcein-labeled areas were clearly longer in both regions after 6 weeks of abaloparatide treatment. Furthermore, the BFR/BS ratio was significantly higher in both the close and distant ROIs 6 weeks after surgery in the abaloparatide group. Taken together, our results suggest that abaloparatide stimulates bone formation with a minimal increase in bone resorption, resulting in greater bone volume following OVX.

This raises the question of how abaloparatide promotes bone formation to surpass resorption. In the OVX+ABL group, the total length of remodeling sites was greater in the close region but not in the distant region, and the total length of modeling sites was significantly elevated in both close and distant ROIs. We hypothesized that abaloparatide-driven anabolic effects can be ascribed not only to remodeling-based bone formation but also to modeling-based bone formation throughout the

metaphyseal trabeculae, as reported by Frost [20] and others [21-24]. Therefore, it seems likely that abaloparatide can induce model-based bone formation with a minimal increase in bone resorption, at least in our mouse model.

Clinical studies in human patients have reported that abaloparatide may have a broader anabolic window than teriparatide [2-4]. Besschetnova et al.. investigated the effects of abaloparatide on bone mass and strength in androgen-deficient orchiectomized rats, a male osteoporosis [25]. They documented increased bone formation on both the periosteal and endosteal surfaces of the cortical bone, and thicker vertebral trabeculae without an increase in osteoclast activity. Similarly, Chandler et al. demonstrated that abaloparatide improved trabecular bone volume and architecture with no increase in osteoclast numbers, using histomorphometry of the tibia [26]. These findings suggest that even under orchiectomized conditions, abaloparatide promotes bone formation with minimal stimulation of bone resorption by osteoclasts. Our findings are consistent with these studies, supporting the conclusion that abaloparatide induces not only remodeling-based bone formation, as teriparatide does, but also modeling-based bone formation.

One might question the molecular mechanisms underlying abaloparatide-driven model-based bone formation. Hattersley et al. demonstrated that when parathyroid hormone (PTH) binds to the R0 conformation of the parathyroid hormone 1 receptor (PTH1R), adenyl cyclase converts ATP to cAMP, leading to a sustained increase in cAMP levels [27]. In contrast, abaloparatide, which selectively binds to the RG conformation of PTH1R, triggers a more transient signaling response characterized by a

307 short and rapid increase in cAMP [27]. This transient signaling mechanism mediated by RG-selective
308 binding could explain the favorable anabolic effects of abaloparatide, including its stimulation of
309 modeling-based bone formation. Recently, using crystal structure analysis, Kobayashi et al. showed
310 that PTH induces prolonged Gs activation, whereas PTHrP induces transient Gs activation [28]. These
311 distinct molecular actions are due to differences in ligand recognition and dissociation kinetics, with a
312 comparison of PTH-bound and PTHrP-bound structures revealing unique ligand–receptor interactions
313 that determine ligand affinity and selectivity. Other investigators postulated that ABL affects the
314 osteocyte transcriptome in a manner subtly different from that of teriparatide, resulting in more
315 beneficial remodeling and modeling of cortical bone [29]. Therefore, it may be possible that osteocytes
316 are involved in modeling-based bone formation induced by abaloparatide. Further examination is
317 necessary to fully understand the effects of abaloparatide on modeling-based bone formation.

318 Administration of abaloparatide at 30 μg/kg once daily for 6 weeks to OVX mice resulted in
319 increased bone mass in the femoral metaphyses, primarily due to enhanced bone formation rather than
320 suppressed bone resorption. Although bone resorption activity was comparable between the OVX and
321 abaloparatide groups, abaloparatide promoted modeling-based bone formation independent of
322 osteoclastic bone resorption.

323

324 **5. Conclusion**

Administration of abaloparatide at 30 μg/kg once daily for 6 weeks to OVX mice resulted in increased bone mass in the femoral metaphyses, primarily due to enhanced bone formation rather than suppressed bone resorption. Although bone resorption activity was comparable between the OVX and abaloparatide groups, abaloparatide promoted modeling-based bone formation independent of osteoclastic bone resorption.

Funding

This work was partially supported by grants from the Japan Society for the Promotion of Science (JSPS, 24K02609 to Amizuka N, 22K0991 to Hasegawa T).

Ethical standards

All animal experiments were performed in accordance with the Japanese Act on Welfare and Management of Animals. The study protocol was approved by the Institutional Animal Care and Use Committee of Hokkaido University (approval no.23-0096).

Competing interests

The authors declare no competing interests.

Contributors

Hasegawa designed the study and reviewed drafts of the research article. Liu X wrote the original draft and analyzed and interpreted the data. Sakakibara M, Shi Y, and Cui J were involved in animal and tissue preparation. Yamamoto T, Haraguchi-Kitakamae M, and Ishizu H performed the histochemical sample preparation, and Hongo H, Li W, and Haoyu W contributed to the bone histomorphometry and statistical analyses. Shimizu T, Ohiro Y, and Amizuka N participated in discussion, editing, and formatting of the manuscript.

Literature Cited

1. Varela A, Chouinard L, Lesage E, Smith SY, Hattersley G. One Year of Abaloparatide, a Selective Activator of the PTH1 Receptor, Increased Bone Formation and Bone Mass in Osteopenic Ovariectomized Rats Without Increasing Bone Resorption. ***J Bone Miner Res.*** 32(1):24-33, 2017.
2. Leder BZ, O'Dea LStL, Zanchetta JR, Kumar P, Banks K, McKay K, et al. Effects of abaloparatide, a human parathyroid hormone-related peptide analog, on bone mineral density in postmenopausal women with osteoporosis. ***J Clin Endocrinol Metab.*** 100(2):697-706, 2015.
3. Miller PD, Hattersley G, Riis BJ, Williams GC, Lau E, Russo LA, et al. Effect of Abaloparatide vs Placebo on New Vertebral Fractures in Postmenopausal Women With Osteoporosis: A Randomized Clinical Trial. ***JAMA.*** 316(7):722-733, 2016.

4. Miller PD, Hattersley G, Lau E, Fitzpatrick LA, Harris AG, Williams GC, et al. Bone mineral density response rates are greater in patients treated with abaloparatide compared with those treated with placebo or teriparatide: Results from the ACTIVE phase 3 trial. ***Bone.*** 120:137-140, 2019.

5. Matsumoto T, Sone T, Yamashita A, Inoue T. Abaloparatide dose-dependently increases bone mineral density in postmenopausal women with osteoporosis: a phase 2 study. *J Bone Miner Metab.* 41(6):807-816, 2023.

6. Dhaliwal R, Kendler D, Saag K, Ing SW, Singer A, Adler RA, et al. Response rates for lumbar spine, total hip, and femoral neck bone mineral density in men treated with abaloparatide: results from the ATOM study. ***JBMR Plus.*** 8(2):ziae009, 2024.

7. Bahar H, Gallacher K, Downall J, Nelson CA, Shomali M, Hattersley G. Six weeks of daily abaloparatide treatment increased vertebral and femoral bone mineral density, microarchitecture and strength in ovariectomized osteopenic rats. ***Calcif Tissue Int.*** 99(5):489-499, 2016.

8. Makino A, Hasegawa T, Yamamoto T, Takagi H, Takahashi Y, Miyakoshi N, et al. Abaloparatide promotes bone repair of vertebral defects in ovariectomized rats by increasing bone formation. ***Bone.*** 182:117056, 2024.

9. Muneyama T, Hasegawa T, Yimin, Yamamoto T, Hongo H, Haraguchi-Kitakamae M, A et al. Histochemical assessment on osteoclasts in long bones of toll-like receptor 2 (TLR2) deficient mice. ***J Oral Biosci.*** 65(2):163-174, 2023.

10. Hasegawa T, Tokunaga S, Yamamoto T, Sakai M, Hongo H, Kawata T, et al. Evocalcet rescues secondary hyperparathyroidism-driven cortical porosity in CKD male rats. ***Endocrinology.*** 164(4):bqad022, 2023.
11. Oda K, Amaya Y, Fukushi-Irie M, Kinameri Y, Ohsuye K, Kubota I, et al. A general method for rapid purification of soluble versions of glycosylphosphatidylinositol-anchored proteins expressed in insect cells: An application for human tissue-nonspecific alkaline phosphatase. ***J. Biochem.*** 126(4):694-9, 1999.
12. Mae T, Hasegawa T, Hongo H, Yamamoto T, Zhao S, Li M, et al. Immunolocalization of enzymes/membrane transporters related to bone mineralization in the metaphyses of the long bones of parathyroid-hormone-administered mice. ***Medicina.*** 59(6):1179, 2023.
13. Hasegawa T, Yamamoto T, Sakai S, Miyamoto Y, Hongo H, Qiu Z, et al. Histological Effects of the Combined Administration of Eldecalcitol and a Parathyroid Hormone in the Metaphyseal Trabeculae of Ovariectomized Rats. ***J Histochem Cytochem.*** 67(3):169-184, 2019.
14. Hasegawa T, Yamamoto T, Hongo H, Yamamoto T, Haraguchi-Kitakamae M, Ishizu H, et al. Eldecalcitol induces minimodeling-based bone formation and inhibits sclerostin synthesis preferentially in the epiphyses rather than metaphyses of long bones in rats. ***Int J Mol Sci.*** 25(8):4257, 2024.

15. Parfitt AM, Drezner MK, Glorieux FH, Kanis JA, Malluche H, Meunier PJ, et al. Bone histomorphometry: standardization of nomenclature, symbols, and units. Report of the ASBMR Histomorphometry Nomenclature Committee. ***J Bone Miner Res.*** 2(6):595-610, 1987.
16. Haraguchi-Kitakamae M, Nakajima Y, Yamamoto T, Hongo H, Cui J, Shi Y, et al. Regional difference in the distribution of alkaline phosphatase, PHOSPHO1, and calcein labeling in the femoral metaphyseal trabeculae in parathyroid hormone-administered mice. ***J Oral Biosci.*** 66(3):554-566, 2024.
17. Houston B, Stewart AJ, Farquharson CF. PHOSPHO1-A novel phosphatase specifically expressed at sites of mineralisation in bone and cartilage. ***Bone.*** 34(4):629-37, 2004.
18. Roberts S, Stewart AJ, Sadler PJ, Farquharson CF. Human PHOSPHO1 exhibits high specific phosphoethanolamine and phosphocholine phosphatase activities. *Biochem J.* 382(Pt 1):59-65, 2004.
19. Roberts S, Narisawa S, Harmey D, Millán JL, Farquharson C. Functional involvement of PHOSPHO1 in matrix vesicle-mediated skeletal mineralization. ***J Bone Miner Res.*** 22(4):617-27, 2007.
20. Frost HM. Micropetrosis. ***J Bone Joint Surg Am.*** 42-A:144-50, 1960.
21. Jee WSS, Tian XY, Setterberg RB. Cancellous bone minimodeling-based formation: a Frost, Takahashi legacy. ***J Musculoskelet Neuronal Interact.*** 7(3):232-9, 2007.

22. Freitas PHL, Hasegawa T, Takeda S, Sasaki M, Tabata C, Oda K, et al. Eldecalcitol, a second-generation vitamin D analog, drives bone minimodeling and reduces osteoclastic number in trabecular bone of ovariectomized rats. ***Bone.*** 49(3):335-42., 2011

23. Sano H, Kondo N, Shimakura T, Fujisawa J, Kijima Y, Knai T, et al. Evidence for Ongoing Modeling-Based Bone Formation in Human Femoral Head Trabeculae via Forming Minimodeling Structures: A Study in Patients with Fractures and Arthritis. ***Front Endocrinol (Lausanne).*** 19:9:88, 2018.

24. Yamamoto T, Hasegawa T, Freitas PHL, Hongo H, Zhao S, Yamamoto T, et al. Histochemical characteristics on minimodeling-based bone formation induced by anabolic drugs for osteoporotic treatment. ***Biomed Res.*** 42(5):161-171, 2021.

25. Besschetnova T, Brooks DJ, Hu D, Nagano K, Nustad J, Ominsky M, et al. Abaloparatide improves cortical geometry and trabecular microarchitecture and increases vertebral and femoral neck strength in a rat model of male osteoporosis. ***Bone.*** 124:148-157, 2019.

26. Chandler H, Lanske B, Varela A, Guillot M, Boyer M, Brown J, et al. Abaloparatide, a novel osteoanabolic PTHrP analog, increases cortical and trabecular bone mass and architecture in orchiectomized rats by increasing bone formation without increasing bone resorption. ***Bone.*** 120:148-155, 2019.

27. Hattersley G, Dean T, Corbin BA, Bahar H, Gardella TJ. Binding Selectivity of Abaloparatide for PTH-Type-1-Receptor Conformations and Effects on Downstream Signaling. ***Endocrinology.*** 157(1):141-9, 2016.

28. Kobayashi K, Kawakami K, Kusakizako T, Miyauchi H, Tomita A, Kobayashi K, et al. Endogenous ligand recognition and structural transition of a human PTH receptor. ***Moe Cell.*** 82(18):3468-3483.e5, 2022.

29. Lv Z, Zhang J, Liang S, Zhou C, Hu D, Brooks DJ, et al. Comparative study in estrogen-depleted mice identifies skeletal and osteocyte transcriptomic responses to abaloparatide and teriparatide. ***JCI Insight.*** 8(20):e161932, 2023.

443 **Figure Legends**

444

445 **Figure 1.** Micro-CT images of femora from the OVX and OVX+ABL groups. Panels A–D are sagittal
446 images of the distal end of femora from mice administered the vehicle (OVX group) at 0, 2, 4, and 6
447 weeks after OVX, while panels E–H show those of OVX mice administered abaloparatide (OVX+ABL
448 group). After administration of the vehicle, a gradual deterioration of metaphyseal trabeculae is
449 apparent (A–D), however, abaloparatide administration reduced metaphyseal trabeculae deterioration
450 (E–H) when compared with OVX group metaphyses under the same treatment period. epi: epiphysis;
451 meta: metaphysis; dia: diaphysis. Bars A-H = 700μm.

452

453

454 **Figure 2.** Histology images and the BV/TV, Tb.Th, Tb.N, and Tb.Sp in the femoral metaphyses from
455 the OVX and OVX+ABL groups. Panels A–D show the femoral metaphyses of OVX mice 0, 2, 4, and
456 6 weeks after the OVX, and panels E–H are highly magnified images of A–D, respectively. Panels I–
457 L display the femoral metaphyses of abaloparatide-administered OVX mice at 0, 2, 4, and 6 weeks,
458 and panels M–P are highly magnified images of I–L, respectively. In the OVX group, the trabecular
459 numbers of femoral metaphyses appear to decrease over time (A–H), while abaloparatide-administered
460 femoral metaphyses remain unchanged (I–P). The values of BV/TV, Tb.Th., and Tb.N are significantly
461 higher in the OVX+ABL group (black bars) compared with the OVX group (white bars) at 2, 4, and 6

462 weeks after the OVX (Q–S). Conversely, Tb.Sp shows significantly lower values in the OVX+ABL
463 group (T). Values are represented as means ± SD, and the significancy of *P*-values is represented using
464 symbols: ### indicates $P < 0.001$ and ## indicates $P < 0.01$ (for Fisher's LSD tests); ††† indicates $P <$
465 0.001, †† indicates $P < 0.01$, and † indicates $P < 0.05$ (for Fisher's LSD tests); and *** indicates $P <$
466 0.01 and ** indicates $P < 0.01$ (for Student's *t*-tests). meta: metaphysis. Bars A-D, I-L = 600μm; bars
467 E-H, M-P = 250μm.
468
469
470 **Figure 3.** Distribution of TRAP-positive/cathepsin K-reactive osteoclasts in femora from the OVX
471 and OVX+ABL groups. Panels A–D show the distribution of TRAP-positive osteoclasts (red color,
472 arrows) in the femoral metaphyses of OVX mice 0, 2, 4, and 6 weeks after the OVX, and panels E–H
473 show the femoral metaphyses of abaloparatide-administered OVX mice (OVX+ABL) at the same
474 treatment periods. Panels I–L show the distribution of cathepsin K-reactive osteoclasts (brown color,
475 arrows) in the femoral metaphyses of OVX mice at 0, 2, 4, and 6 weeks, and panels M–P show the
476 femoral metaphyses of abaloparatide-administered OVX mice (OVX+ABL) at the same treatment
477 periods. Panels Q and R show the means ± SD and statistical analysis results for TRAP-Oc.N/TV
478 and TRAP-Oc.N/BS at 0, 2, 4, and 6 weeks in the OVX (white bars) and OVX+ABL (black bars)
479 groups, while panels S and T show those for Cat K-Oc.N/TV and Cat K-Oc.N/BS. The significancy of
480 *P*-values is represented using symbols: ### indicates $P < 0.001$, ## indicates $P < 0.01$, and # indicates *P*

481 < 0.05 (for Fisher's LSD tests); ††† indicates $P < 0.001$, †† indicates $P < 0.01$, and † indicates $P < 0.05$

482 (for Fisher's LSD tests); and *** indicates $P < 0.01$, ** indicates $P < 0.01$, and * indicates $P < 0.05$

483 (for Student's *t*-tests). meta: metaphysis. Bars A-P = 200 μm.

484

485

486 **Figure 4.** Distribution of ALP-positive osteoblasts in femora from the OVX and OVX+ABL groups.

487 Panels A–D show the distribution of ALP-positive cells (brown color) in the femoral metaphyses of

488 OVX mice 0, 2, 4, and 6 weeks after the OVX, and panels E–H are highly magnified images of A–D,

489 respectively. Similarly, panels I–L display the distribution of ALP-positive cells in the femoral

490 metaphyses of abaloparatide-administered OVX mice (OVX+ABL) at 0, 2, 4, and 6 weeks, and panels

491 M–P are highly magnified images of I–L. Panels Q and R represent the means ± SD and statistical

492 analysis results for ALP+area/TV and ALP+area/BV at 0, 2, 4, and 6 weeks in the OVX (white bars)

493 and OVX+ABL (black bars) groups. The significancy of *P*-values is represented using symbols: $^{\#\#\#}$

494 indicates $P < 0.001$, $^{\#\#}$ indicates $P < 0.01$, and $^{\#}$ indicates $P < 0.05$ (for Fisher's LSD tests); ††† indicates

495 $P < 0.001$, †† indicates $P < 0.01$, and † indicates $P < 0.05$ (for Fisher's LSD tests); and *** indicates P

496 < 0.01, ** indicates $P < 0.01$, and * indicates $P < 0.05$ (for Student's *t*-tests). meta: metaphysis. Bars

497 A-D, I-L = 300 μm; bars E-H, M-P = 200μm

498

499

Figure 5. Distribution of PHOSPHO1-reactive osteoblasts in femora from the OVX and OVX+ABL groups. Panels A–D show the distribution of PHOSPHO1-reactive osteoblasts (brown color) in the femoral metaphyses of OVX mice at 0, 2, 4, and 6 weeks, and panels E–H are highly magnified images of A–D, respectively. Similarly, panels I–L display the distribution of PHOSPHO1-reactive osteoblasts in abaloparatide-administered OVX mice at the same treatment periods, and panels M–P are highly magnified images of I–L. In the OVX group, PHOSPHO1-reactive osteoblasts (arrows) become more localized towards the chondro-osseous junction over time (E–H), whereas in the OVX+ABL group, many rows of PHOSPHO1-reactive mature osteoblasts (arrows) are observed throughout the metaphyseal trabeculae (M–P). Panels Q and R display the means ± SD and statistical analysis results forPHOSPHO1+area/TV and PHOSPHO1+area/BV at 0, 2, 4, and 6 weeks in the OVX (white bars) and OVX+ABL (black bars) groups. The significancy of *P*-values is represented using symbols: $^{\#\#\#}$ indicates $P < 0.001$ and $^{\#}$ indicates $P < 0.05$ (for Fisher's LSD tests); ††† indicates $P < 0.001$, †† indicates $P < 0.01$, and † indicates $P < 0.05$ (for Fisher's LSD tests); and *** indicates $P < 0.01$, ** indicates $P < 0.01$, and * indicates $P < 0.05$ (for Student's *t*-tests). meta: metaphysis. Bars A-D, I-L = 300 μm; bars E-H, M-P = 200 μm.

Figure 6. Calcein labeling in the femoral metaphyses of the OVX and OVX+ABL groups. Panels A and B show low-magnification images of the femoral metaphyses of the OVX (A) and OVX+ABL (B)

519 group. Note close and distant assumed boxed areas, regions of interest (ROI), represented by dotted
520 lines. Panels C–E and I–K depict calcein labeling in the close and distant ROIs, respectively, of the
521 OVX group at 0, 2, and 6 weeks, while panels F–H and L–N show the close and distant ROIs of the
522 OVX+ABL group. Note that the close region of OVX+ABL group contains many, long lines of calcein
523 labeling at 2 and 6 weeks, while much fewer and shorter lines are seen in the OVX group. In addition,
524 at 2 and 6 weeks, there are many more continuous, long calcein labels in the distant region of the
525 OVX+ABL group (M, N) compared to that of the OVX group (J, K). meta: metaphysis, dia: diaphysis.
526 Bars A, B = 500 μm; bars C-N = 200 μm.
527
528
529 **Figure 7.** Means ± SD and statistical analysis results for the average length of calcein labeling and
530 BFR/BS at 0, 2, and 6 weeks and the total length of remodeling and modeling sites at 0 and 6 weeks
531 in femora from the OVX and OVX+ABL groups. Panels A and B represent the average length of
532 calcein labeling in the close (A) and distant regions (B), while panels C and D reveal BFR/BS in the
533 close (C) and distant regions (D). The total lengths of remodeling sites 6 weeks post-operation are
534 shown in panels E (proximal region) and F (distal region). Similarly, the total length of modeling sites
535 at 6 weeks post-operation are presented in panels G (proximal region) and H (distal region). The
536 significancy of *P*-values is represented using symbols: $^{\#\#}$ indicates $P < 0.01$ and $^{\#}$ indicates $P < 0.05$
537 (for Fisher's LSD tests); ††† indicates $P < 0.001$, †† indicates $P < 0.01$, and † indicates $P < 0.05$ (for

538 Fisher's LSD tests); and *** indicates $P < 0.01$, ** indicates $P < 0.01$, and * indicates $P < 0.05$ (for

539 Student's *t*-tests).

540

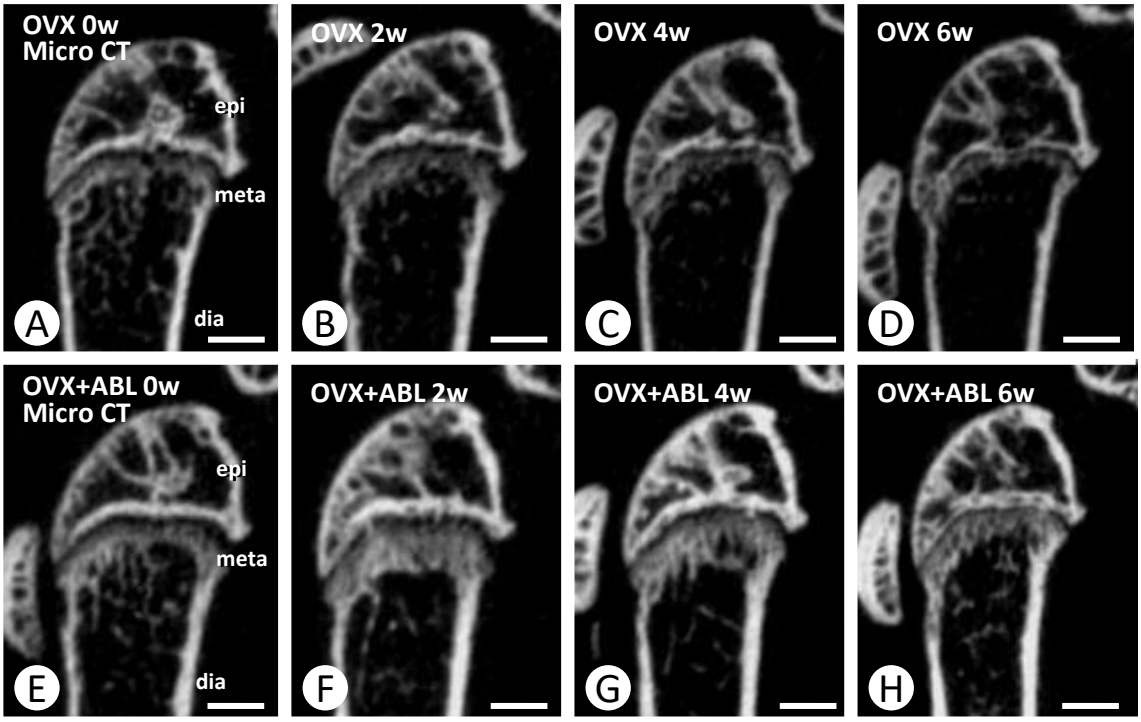
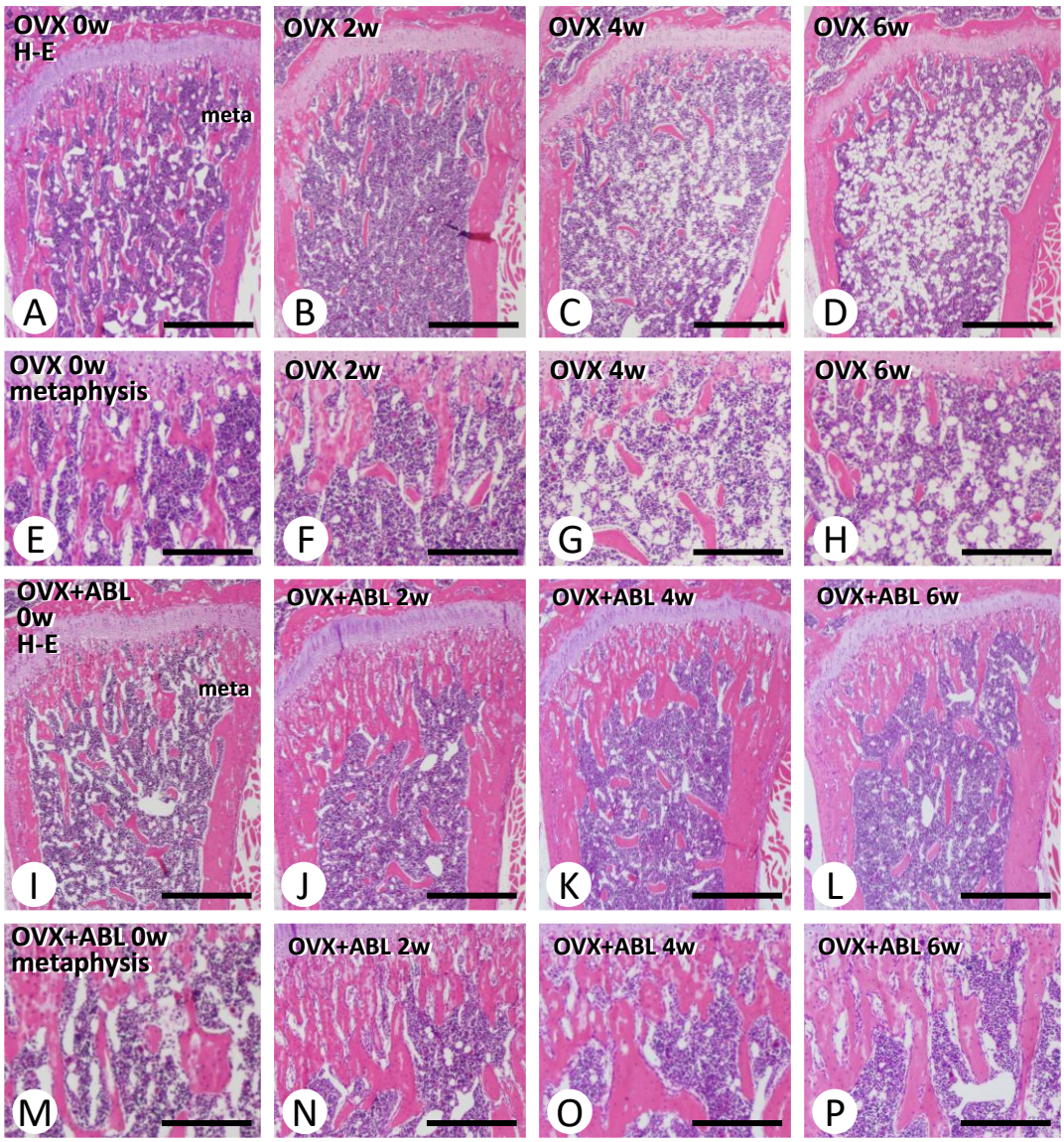

OVX 0w
Micro CT
epi
meta
dia
A
OVX 2w
B
OVX 4w
C
OVX 6w
D
OVX+ABL 0w
Micro CT
epi
meta
dia
E
OVX+ABL 2w
F
OVX+ABL 4w
G
OVX+ABL 6w
H

Figure 1


OVX 0w
H-E
meta
A
OVX 2w
B
OVX 4w
C
OVX 6w
D
OVX 0w
metaphysis
E
OVX 2w
F
OVX 4w
G
OVX 6w
H
OVX+ABL
0w
H-E
meta
I
OVX+ABL 2w
J
OVX+ABL 4w
K
OVX+ABL 6w
L
OVX+ABL 0w
metaphysis
M
OVX+ABL 2w
N
OVX+ABL 4w
O
OVX+ABL 6w
P

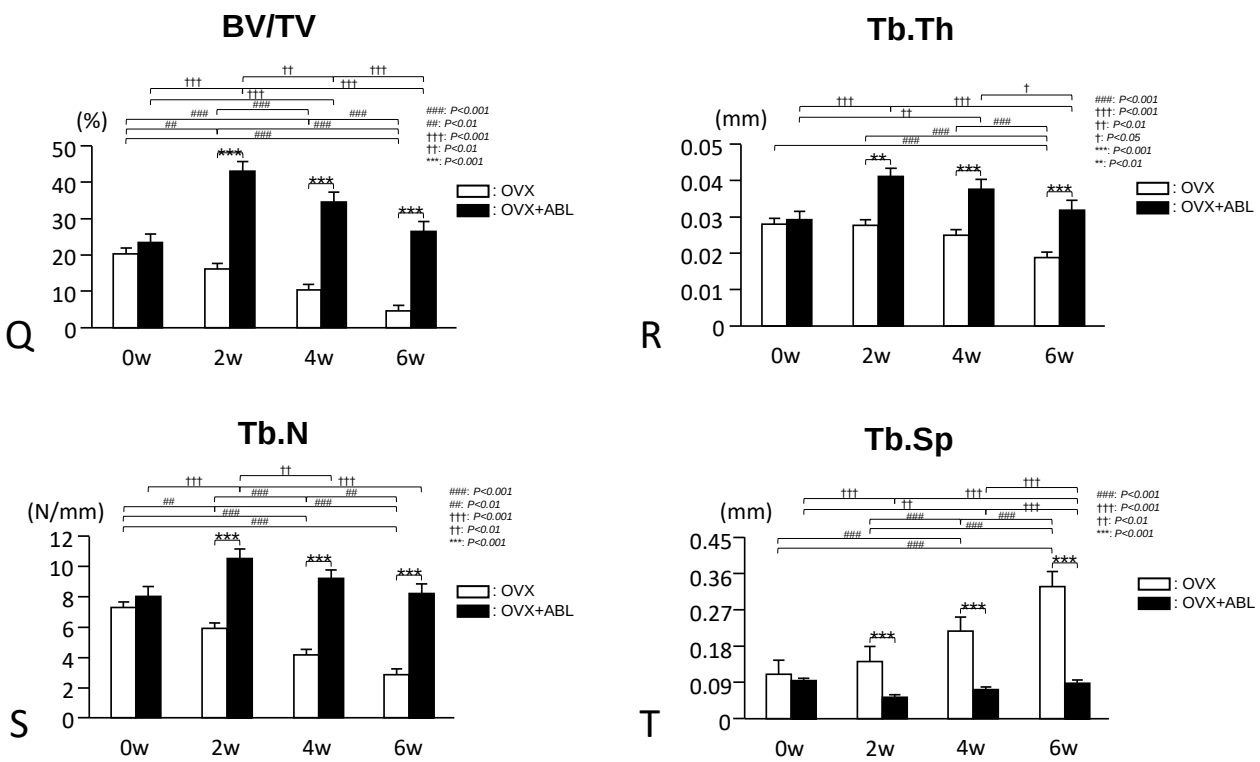
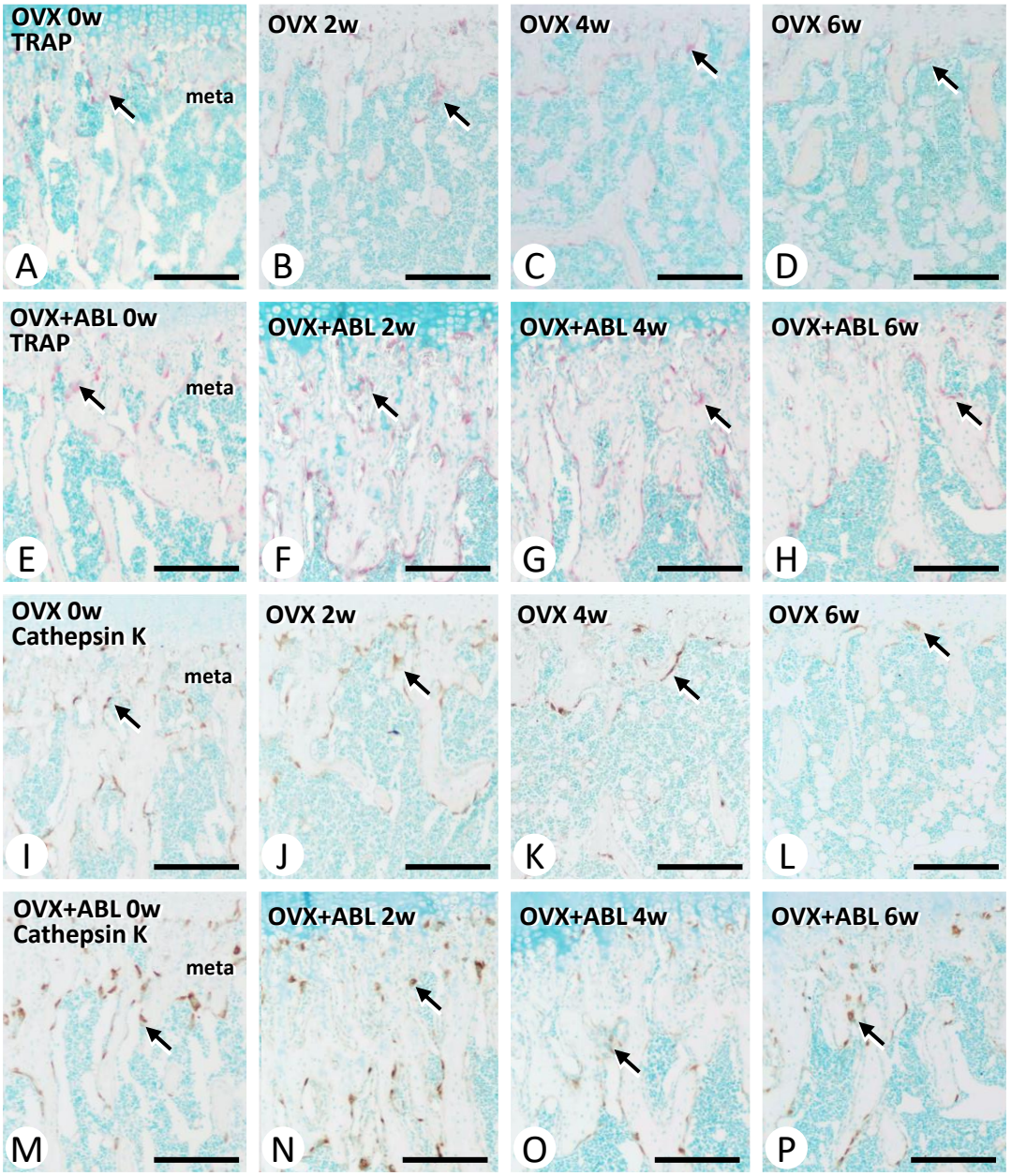
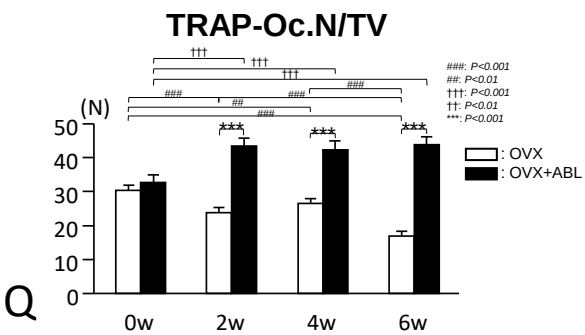
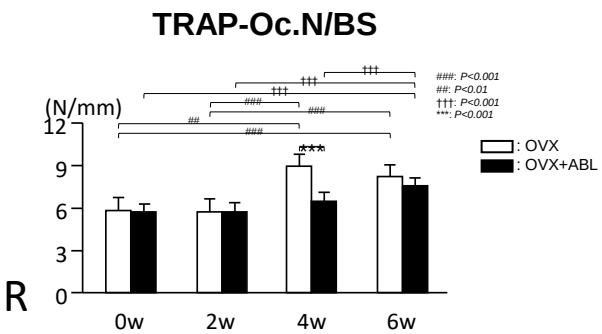

BV/TV
(%)
50
40
30
20
10
0
0w
2w
4w
6w
###: P<0.001
##: P<0.01
†††: P<0.001
††: P<0.01
***: P<0.001
: OVX
: OVX+ABL
Q
Tb.Th
(mm)
0.05
0.04
0.03
0.02
0.01
0
†: P<0.05
**: P<0.01
R
Tb.N
(N/mm)
12
10
8
6
4
2
S
Tb.Sp
0.45
0.36
0.27
0.18
0.09
T

Figure 2

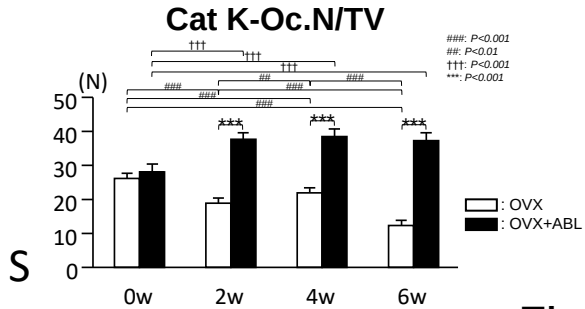




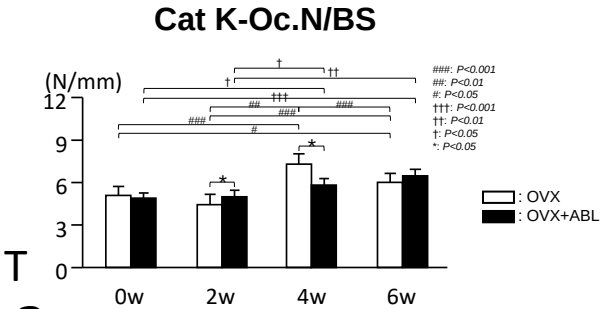
Q



R

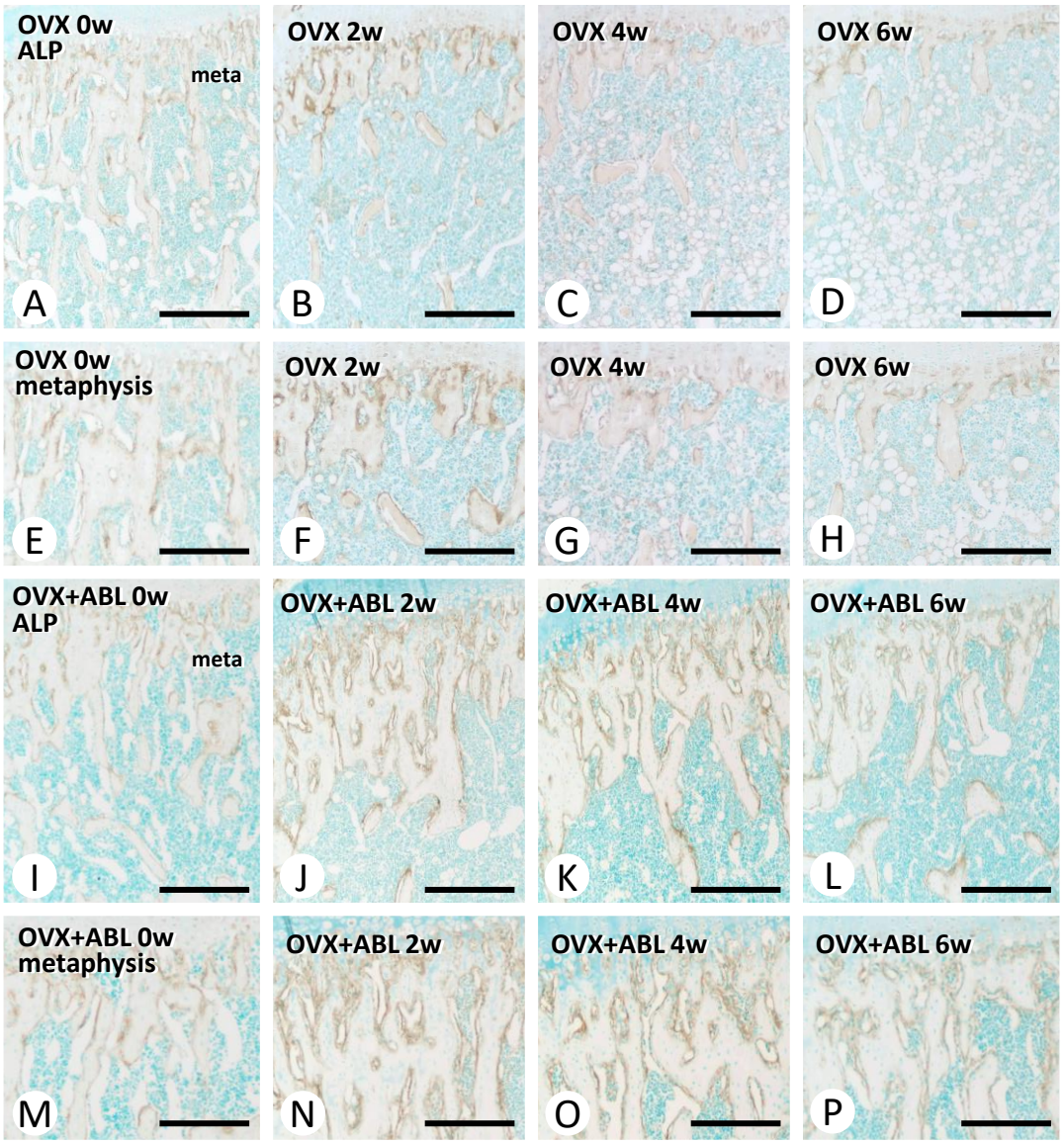


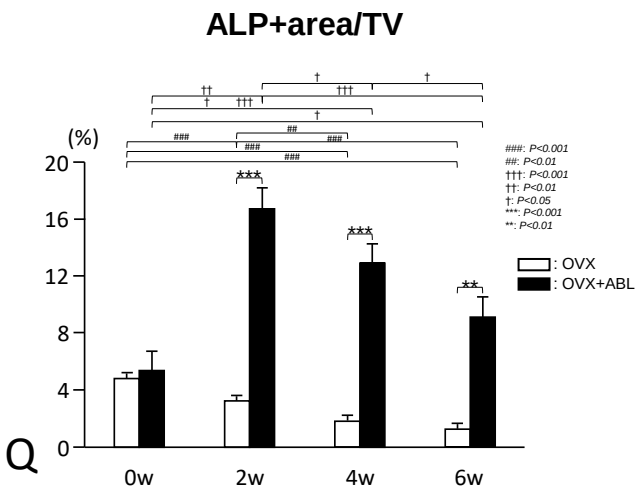
S



T

Figure 3


OVX 0w
ALP
meta
A
OVX 2w
B
OVX 4w
C
OVX 6w
D
OVX 0w
metaphysis
E
OVX 2w
F
OVX 4w
G
OVX 6w
H
OVX+ABL 0w
ALP
meta
I
OVX+ABL 2w
J
OVX+ABL 4w
K
OVX+ABL 6w
L
OVX+ABL 0w
metaphysis
M
OVX+ABL 2w
N
OVX+ABL 4w
O
OVX+ABL 6w
P


ALP+area/TV
(%)
20
16
12
8
4
0
0w
2w
4w
6w
###: P<0.001
##: P<0.01
†††: P<0.001
††: P<0.01
†: P<0.05
***: P<0.001
**: P<0.01
: OVX
: OVX+ABL
Q

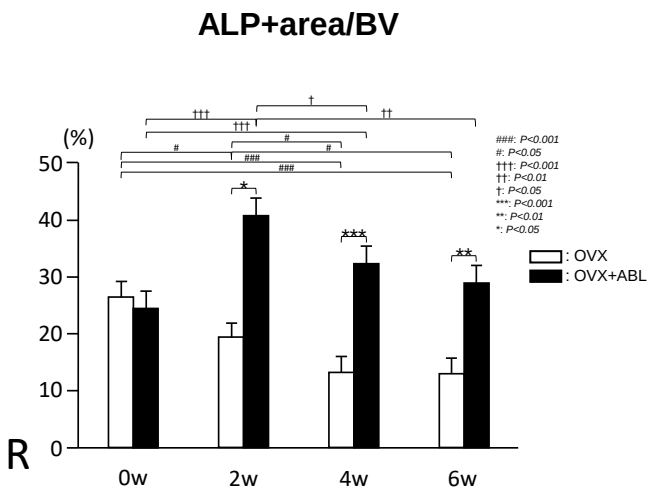
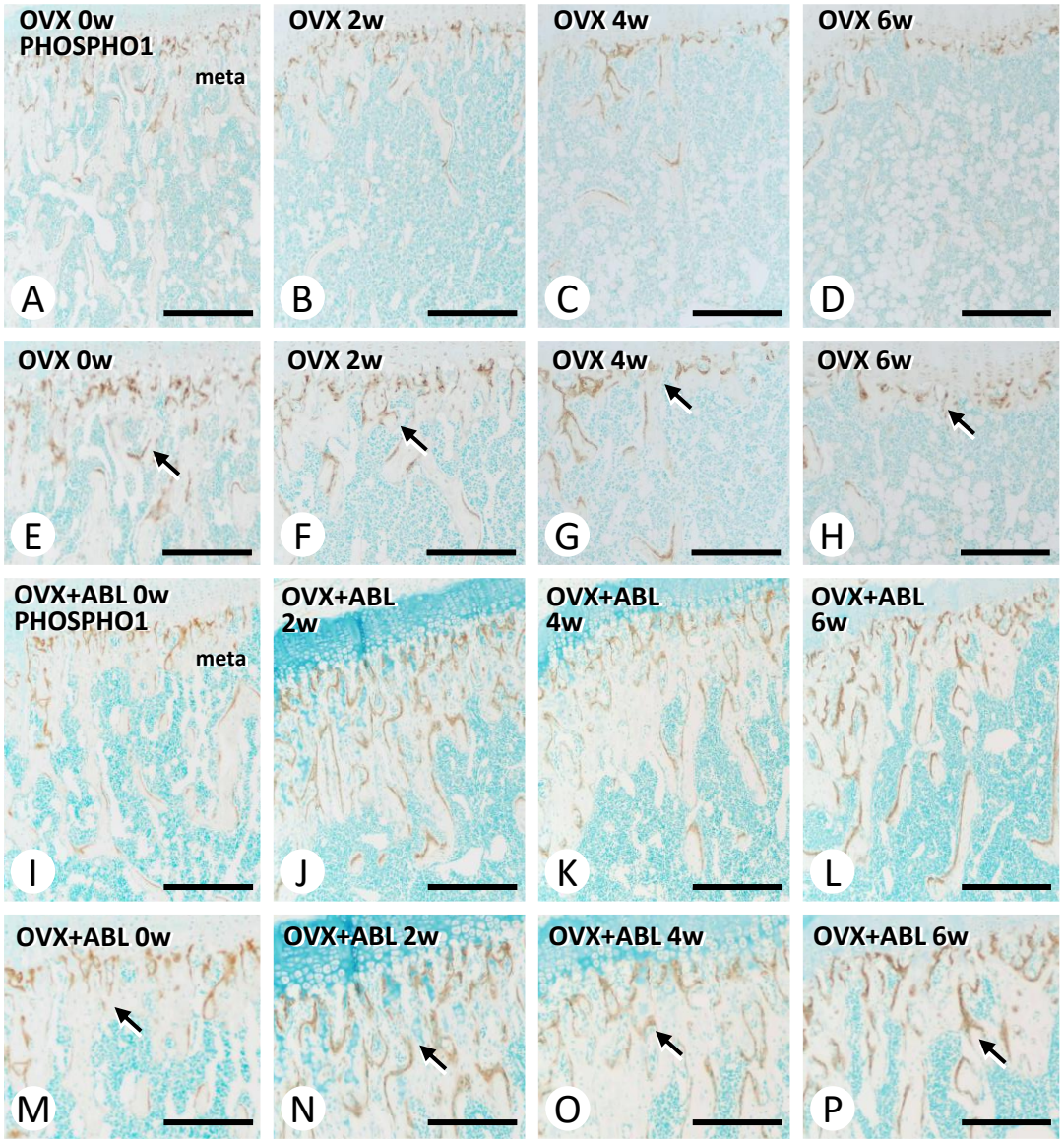
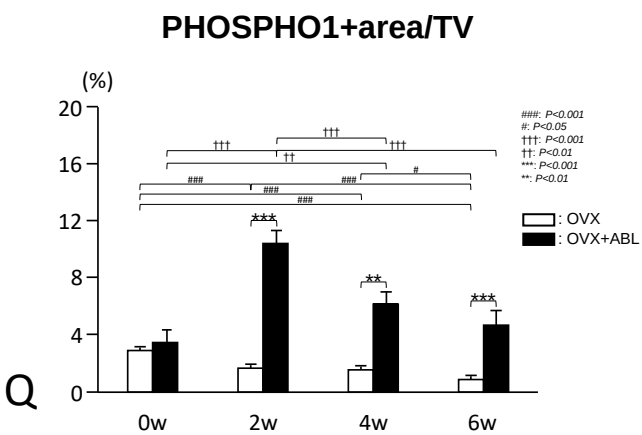
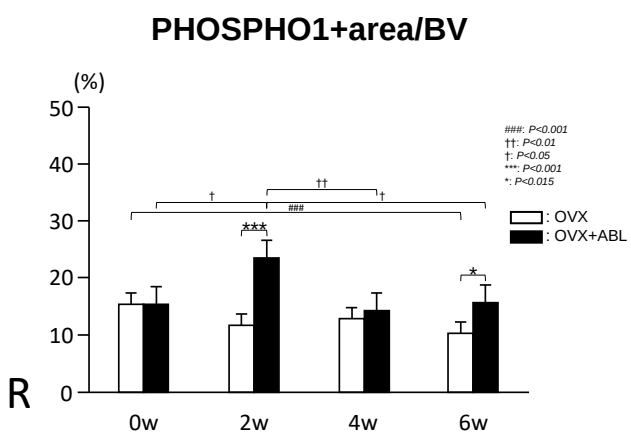

ALP+area/BV
(%)
50
40
30
20
10
0
0w
2w
4w
6w
###: P<0.001
#: P<0.05
†††: P<0.001
††: P<0.01
†: P<0.05
***: P<0.001
**: P<0.01
*: P<0.05
: OVX
: OVX+ABL
R

Figure 4


OVX 0w
PHOSPHO1
meta
A
OVX 2w
B
OVX 4w
C
OVX 6w
D
OVX 0w
E
OVX 2w
F
OVX 4w
G
OVX 6w
H
OVX+ABL 0w
PHOSPHO1
meta
I
OVX+ABL
2w
J
OVX+ABL
4w
K
OVX+ABL
6w
L
OVX+ABL 0w
M
OVX+ABL 2w
N
OVX+ABL 4w
O
OVX+ABL 6w
P


PHOSPHO1+area/TV
(%)
20
16
12
8
4
0
0w
2w
4w
6w
###: P<0.001
#: P<0.05
†††: P<0.001
††: P<0.01
***: P<0.001
**: P<0.01
: OVX
: OVX+ABL

Q


PHOSPHO1+area/BV
(%)
50
40
30
20
10
0
0w
2w
4w
6w
###: P<0.001
††: P<0.01
†: P<0.05
***: P<0.001
*: P<0.015
: OVX
: OVX+ABL

R

Figure 5

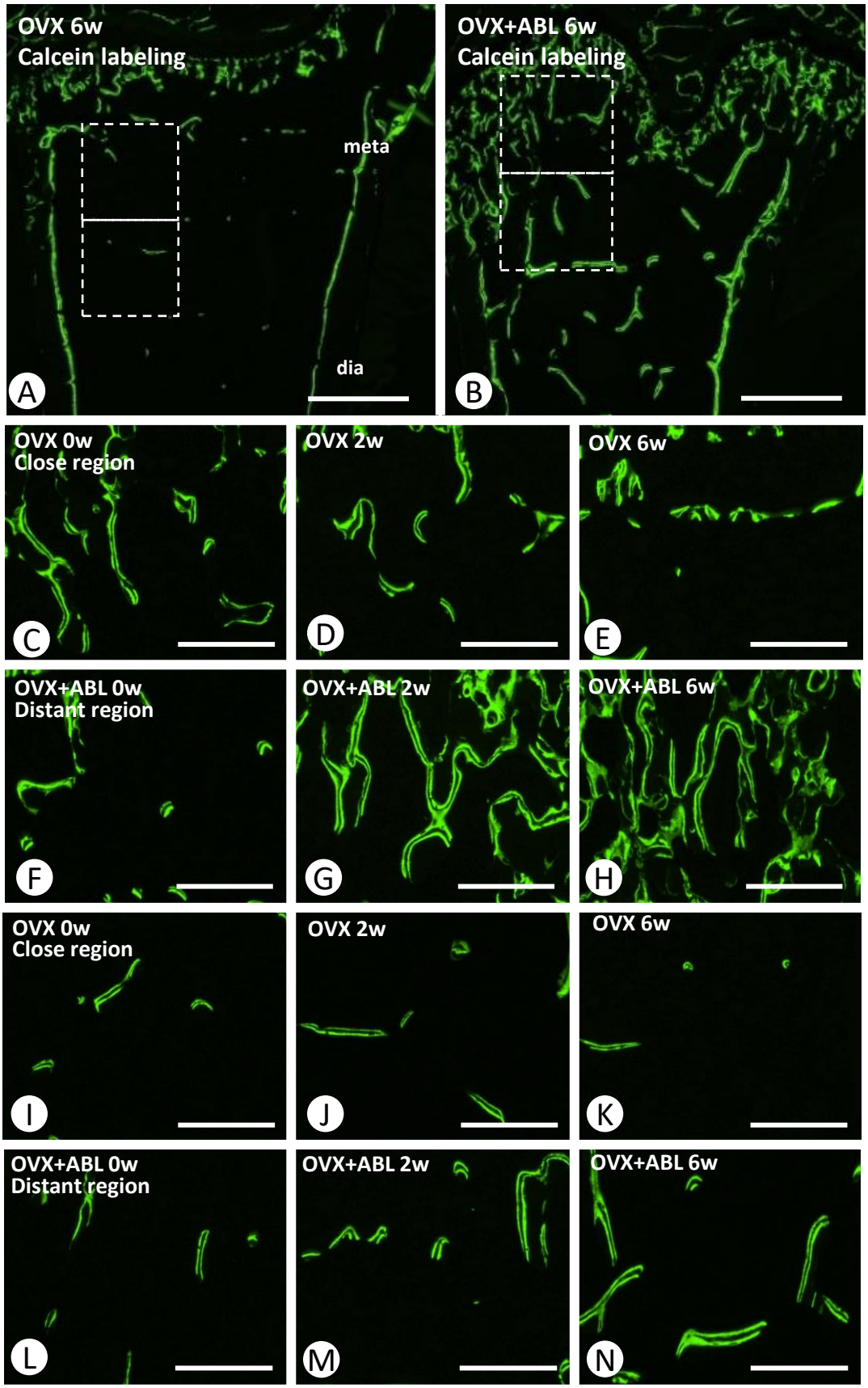

OVX 6w
Calcein labeling
meta
dia
A
OVX+ABL 6w
Calcein labeling
B
OVX 0w
Close region
C
OVX 2w
D
OVX 6w
E
OVX+ABL 0w
Distant region
F
OVX+ABL 2w
G
OVX+ABL 6w
H
OVX 0w
Close region
I
OVX 2w
J
OVX 6w
K
OVX+ABL 0w
Distant region
L
OVX+ABL 2w
M
OVX+ABL 6w
N

Figure 6

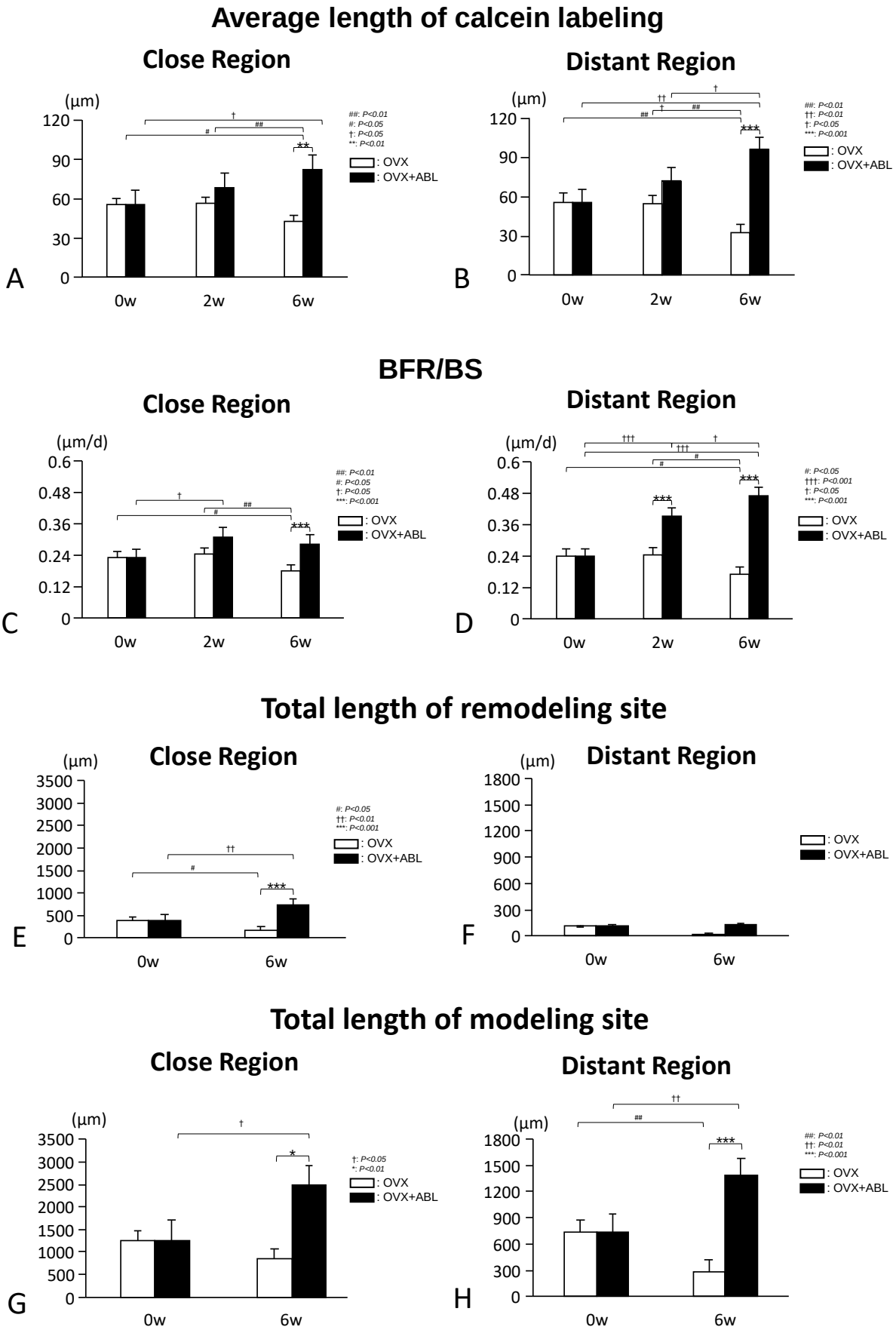

Average length of calcein labeling
Close Region
Distant Region
A
B
(μm)
120
90
60
30
0
0w
2w
6w
##: P<0.01
#: P<0.05
†: P<0.05
**: P<0.01
††: P<0.01
***: P<0.001
: OVX
: OVX+ABL
BFR/BS
C
D
(μm/d)
0.6
0.48
0.36
0.24
0.12
†††: P<0.001
Total length of remodeling site
E
F
3500
3000
2500
2000
1500
1000
500
1800
1200
900
600
300
Total length of modeling site
G
H
*: P<0.01

Figure 7